

Axial charges of octet and decuplet baryons in a perturbative chiral quark model

X. Y. Liu,^{1,2,*} D. Samart,^{3,2,†} K. Khosonthongkee,^{2,‡} A. Limphirat,² K. Xu,² and Y. Yan²

¹School of Mathematics and Physics, Bohai University, Jinzhou 121013, China

²School of Physics and Center of Excellence in High Energy Physics and Astrophysics, Suranaree University of Technology, Nakhon Ratchasima 30000, Thailand

³Department of Applied Physics, Faculty of Sciences and Liberal Arts, Rajamangala University of Technology Isan, Nakhon Ratchasima 30000, Thailand

(Received 9 October 2017; revised manuscript received 5 April 2018; published 9 May 2018)

Using the perturbative chiral quark model (PCQM), we investigate and predict in this work axial charges g_A^B of octet and decuplet N , Σ , Ξ , Δ , Σ^* , and Ξ^* baryons, considering both the ground and excited states in the quark propagator. The PCQM predictions are in good agreement with the experimental data, lattice-QCD values, and other approaches. In addition, the study reveals that the meson cloud is influential in the PCQM, contributing around 30% to the total values of g_A^B , and the meson cloud contribution to g_A^B stems mainly from the diagrams with the ground-state quark propagator while the excited intermediate quark states reduce g_A^B by 10–20%.

DOI: [10.1103/PhysRevC.97.055206](https://doi.org/10.1103/PhysRevC.97.055206)

I. INTRODUCTION

The axial charge of a baryon g_A^B , which is defined as a value of axial form factor at zero recoil, is a very important parameter for the understanding of the baryon electroweak structures and interactions and has been of interest for many years. Among them all, the nucleon axial charge g_A^N is best known and is reported experimentally as $g_A^N = 1.2723 \pm 0.0023$ [1]. The nucleon axial charge g_A^N governs the neutron β decay and it is also a basic ingredient of the spontaneous breaking of chiral symmetry. Theoretically, the nucleon axial charge g_A^N has been evaluated in various approaches [2–17] and the theoretical results are found to be in good agreement with the experimental value. More experimental and theoretical reviews on the nucleon axial charge g_A^N can be found in Refs. [18–20].

Except for the nucleon, unfortunately, there is no direct experimental data for other baryons. In recent years, the axial charges of hyperons have been “measured” in lattice QCD [21–25], and these lattice QCD values may be identified as reliable evidence when experimental data are scarce. Meanwhile, the hyperon axial charges have been predicted in chiral perturbation theory (ChPT) [26–32], QCD sum rule [33], and various quark models [34–39]. In Refs. [40,41], the predictions of axial charges of the octet and decuplet baryons as well as their resonances have also been given by the relativistic constituent quark model (RCQM) with including extended Goldstone boson-exchange (EGBE) and one-gluon-exchange (OGE) quark-quark interactions. Thus the success of such calculations inspires us to study the axial couplings for the octet and decuplet baryons in the perturbative chiral quark model (PCQM).

The PCQM is one of the effective approaches within the low-energy particle physics and has been successfully applied to study the structure and properties of baryons [42–57]. In our previous work [56], we have determined the ground-state quark wave function in the PCQM by fitting the theoretical result of the proton charge form factor $G_E^p(Q^2)$ to the experimental data, and the PCQM results of the octet baryon electroweak form factors based on the predetermined ground-state quark wave function are fairly consistent with the experimental data and lattice QCD values [56,57]. That may indicate that the predetermined ground-state quark wave function is reasonable and credible in the PCQM. Furthermore, a Cornell-like potential of the PCQM is extracted in accordance with the predetermined ground-state quark wave function in our recent works [58,59], and the excited quark states are derived numerically. The neutron charge form factor is evaluated in the PCQM considering both the ground and excited states in the quark propagator [58]. The results reveal that the excited states in the quark propagator are considerably influential in the charge form factor and charge radius of neutron. In addition, Refs. [47,48] also report that the excited quark propagators increase the contribution of the loop diagrams around 10% in comparison to the $3q$ -core diagram in the PCQM. Therefore, we attempt to investigate and predict in this work the axial charges of the octet and decuplet N , Σ , Ξ , Δ , Σ^* , and Ξ^* baryons in the framework of the PCQM considering both the ground and excited states in the quark propagator.

The paper is organized as follows. In Sec. II, we introduce the PCQM with the ground- and excited-state quark wave functions. The numerical results on the octet and decuplet baryon axial charges and discussion are given in Sec. III. Finally, we summarize and conclude the work in Sec. IV.

II. PERTURBATIVE CHIRAL QUARK MODEL

The PCQM is an effective chiral Lagrangian describing three relativistic valence quarks of baryons moving in a

*lxy_gzu2005@126.com

†daris.sa@rmuti.ac.th

‡khanchai@g.sut.ac.th

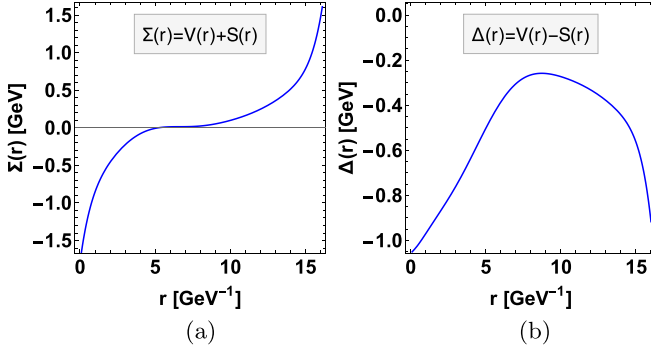


FIG. 1. The extracted PCQM potentials based on the predetermined ground-state quark wave function: $\Sigma(r)$ potential (a) and $\Delta(r)$ potential (b).

central potential $V_{\text{eff}}(r) = S(r) + \gamma^0 V(r)$, and the interactions between quarks and pseudoscalar mesons are achieved by the nonlinear σ model in the PCQM. The Weinberg-type Lagrangian of the PCQM under an unitary chiral rotation [56,57] is derived as

$$\mathcal{L}_0(x) = \bar{\psi}(x)[i\cancel{d} - \gamma^0 V(r) - S(r)]\psi(x) - \frac{1}{2}\Phi_i(x)(\square + M_\Phi^2)\Phi^i(x), \quad (1)$$

$$\mathcal{L}_I^W(x) = \frac{1}{2F}\partial_\mu\Phi_i(x)\bar{\psi}(x)\gamma^\mu\gamma^5\lambda^i\psi(x), \quad (2)$$

where the pion decay constant $F = 88$ MeV in the chiral limit, Φ_i are the octet meson fields, and $\psi(x)$ is the triplet of the u , d , and s quark fields taking the form

$$\psi(x) = \begin{pmatrix} u(x) \\ d(x) \\ s(x) \end{pmatrix}. \quad (3)$$

The quark field $\psi(x)$ could be expanded in the form

$$\psi(x) = \sum_\alpha (b_\alpha u_\alpha(\vec{x}) e^{-iE_\alpha t} + d_\alpha^\dagger v_\alpha(\vec{x}) e^{iE_\alpha t}), \quad (4)$$

with b_α and d_α^\dagger being the single quark annihilation and antiquark creation operators, and u_α and v_β are the set of quark and antiquark wave functions in orbits α and β .

In general, the quark wave functions $u_\alpha(\vec{x})$ may be expressed as

$$u_\alpha(\vec{x}) = \begin{pmatrix} g_\alpha(r) \\ i\vec{\sigma} \cdot \hat{x} f_\alpha(r) \end{pmatrix} \chi_s \chi_f \chi_c, \quad (5)$$

where χ_s , χ_f , and χ_c are the spin, flavor, and color quark wave functions, respectively, and must satisfy the static Dirac equation with the central potentials $V(r)$ and $S(r)$,

$$[-i\gamma^0\gamma \cdot \nabla + \gamma^0 S(r) + V(r) - E_\alpha]u_\alpha(x) = 0, \quad (6)$$

where E_α is the single quark energy.

In our previous work [58,59], the PCQM potentials $\Sigma(r) = V(r) + S(r)$ and $\Delta(r) = V(r) - S(r)$ presented in Fig. 1 have been extracted by letting the predetermined ground-state quark wave function $u_0(\vec{x})$ satisfy Dirac equation (6) with considering the quark confinement and asymptotic freedom properties as

boundary conditions. As shown in Fig. 1(a), the potential $\Sigma(r)$ presents a Cornell-like potential pattern. The potential $\Sigma(r)$ takes the form of Coulomb potential at small r but goes up quickly to infinite with r increasing, which may be understood as the quark confinement. At the middle region of r , the potential $\Sigma(r)$ is nearly zero, which may indicate quarks are more or less free. The potential $\Delta(r)$ in Fig. 1(b) results in a mass well.

Moreover, we derive the ground and excited quark wave functions by solving Eq. (6) with the extracted PCQM potentials numerically in terms of generalized eigenvalue and eigenstate problem method,

$$H_{n'n}C_n = E_\alpha D_{n'n}C_n, \quad (7)$$

$$H = \begin{pmatrix} E_0 + \Sigma(r) & -\frac{d}{dr} + \kappa/r \\ \frac{d}{dr} + \kappa/r & E_0 + \Delta(r) \end{pmatrix}. \quad (8)$$

In the numerical calculation, the radial quark wave functions, the upper $g_\alpha(r)$ and lower $f_\alpha(r)$ components, are expanded in the complete set of Sturmian functions $S_{nl}(r)$ [56],

$$g_\alpha(r) = \sum_n A_n S_{nl}(r), \quad (9)$$

$$f_\alpha(r) = \sum_n B_n S_{nl}(r), \quad (10)$$

with

$$S_{nl}(r) = \left[\frac{n!}{(n+2l+1)!} \right]^{\frac{1}{2}} (2br)^{l+1} e^{-br} L_n^{2l+1}(2br), \quad (11)$$

where $L_n^{2l+1}(x)$ are Laguerre polynomials, and b is the length parameter of Sturmian functions. $H_{n'n}$ in Eq. (7) are the matrix elements of operator H of Eq. (8) in the Sturmian basis, and $D_{n'n} = \langle S_{n'l}(r) | S_{nl}(r) \rangle$. For a given total angular momentum j , the spin-orbit coupling quantum number κ in Eq. (8) is taken as $\kappa = j + \frac{1}{2}$ if the orbit angular momentum $l = j - \frac{1}{2}$, and $\kappa = -(j + \frac{1}{2})$ if $l = j + \frac{1}{2}$. In Eq. (7), E_α and C_n are the eigenvalues and eigenstates, respectively, and C_n is taken form as a column vector $(A_1, \dots, A_n, B_1, \dots, B_n)^T$. The ground-state quark energy E_0 is a free parameter and has been determined by fitting the PCQM result of nucleon mass to the experimental value as $E_0 = 0.524$ GeV in Ref. [59].

In Table I, we list the numerical results of energy levels of a single quark E_α with $E_0 = 0.524$ GeV. Also, the radial wave functions of the valence quarks are presented in Fig. 2 with the upper component $g(r)$ and the lower component $f(r)$. In the PCQM, the energy levels E_α are restricted up to the low-energy scalar $\Lambda = 1$ GeV. Therefore, the ground state $1s_{1/2}$ and the excited states $1p_{1/2}$, $1p_{3/2}$, $1d_{3/2}$, $1d_{5/2}$, $1f_{5/2}$, $1f_{7/2}$, $2s_{1/2}$, $2p_{1/2}$, $2p_{3/2}$, and $3s_{1/2}$ as shown in Figs. 2(a)-2(k) could be included in the quark propagator to investigate the axial charges of the octet and decuplet baryons in this work. It is noted that the quark wave functions are normalized according to $\int d^3\vec{x} u_\alpha^\dagger(\vec{x}) u_\alpha(\vec{x}) = 1$. For details of the PCQM potentials and quark wave functions, we refer to Refs. [59].

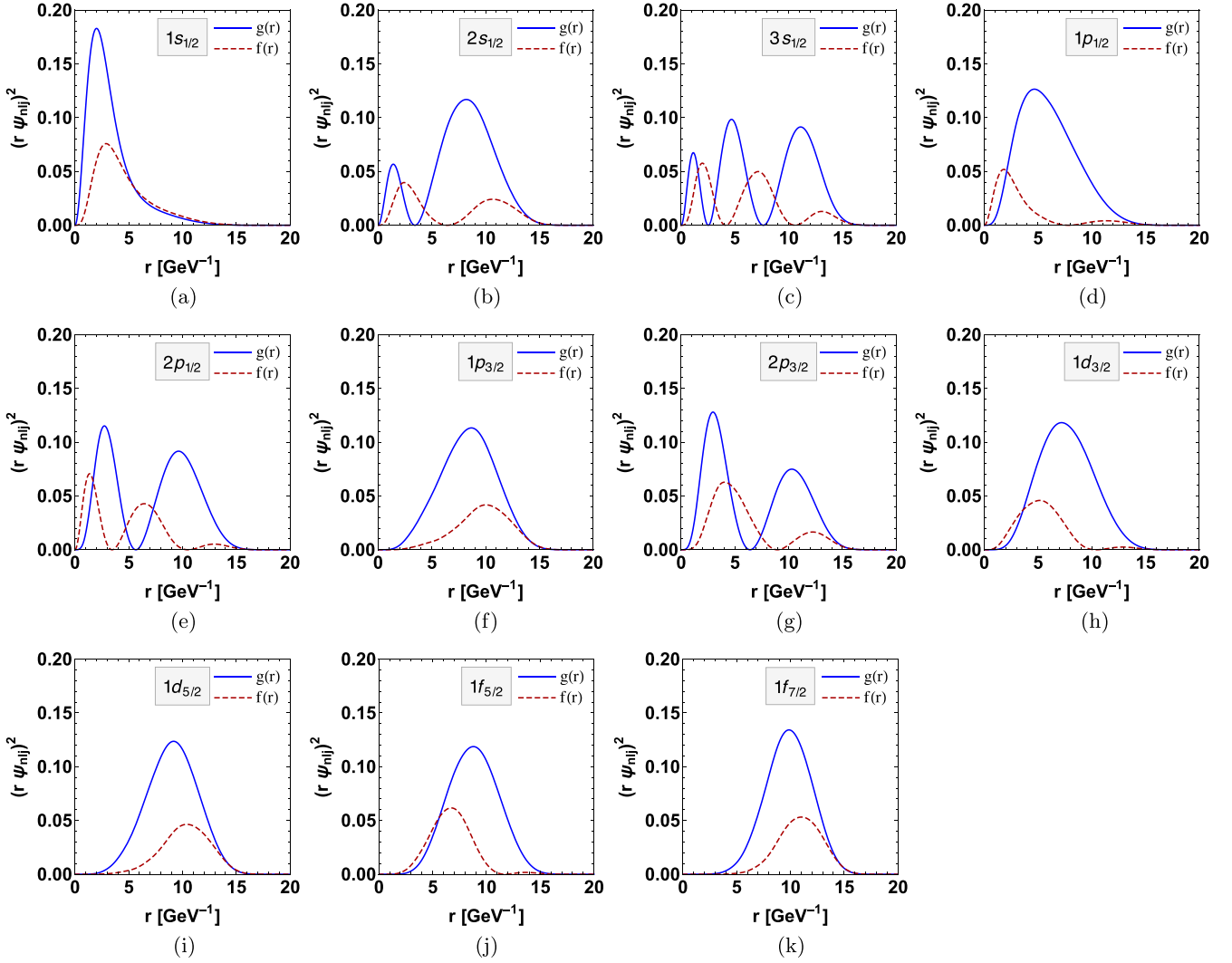


FIG. 2. The numerical results on the normalized radial wave functions of the valence quarks for the upper component $g(r)$ and the lower component $f(r)$.

III. AXIAL CHARGES OF OCTET AND DECUPLET BARYONS IN PCQM

The baryon axial charge g_A^B is a value of the axial form factor $G_A^B(Q^2)$ at the limit $Q^2 = 0$, and is defined within the PCQM up to the one-loop order as

$$\begin{aligned} & \chi_{B_s}^\dagger \vec{\sigma}_B \frac{\tau_B^3}{2} \chi_{B_s} g_A^B \\ &= {}^B \langle \phi_0 | \sum_{n=0}^2 \frac{i^n}{n!} \int \delta(t) d^4 x d^4 x_1 \dots d^4 x_n e^{-i E_\alpha t} \\ & \quad \times T[\mathcal{L}_I^W(x_1) \dots \mathcal{L}_I^W(x_n) \vec{A}_3(x)] |\phi_0 \rangle^B. \end{aligned} \quad (12)$$

Here, χ_{B_s} and $\chi_{B_s}^\dagger$ are the baryon spin wave functions in the initial and final states. $\vec{\sigma}_B$ is the baryon spin matrix and τ_B^3 is the third component of the isospin matrix of the baryon. The state vectors $|\phi_0\rangle^B$ correspond to the unperturbed three-quark states projected onto the baryon states. For one-body operators, the

projection is

$$\chi_{f'}^\dagger \chi_{s'}^\dagger I^{f'f} J^{s's} \chi_s^\dagger \chi_f^\dagger \xrightarrow{\text{Proj.}} \langle B | \sum_{i=1}^3 (IJ)^{(i)} | B \rangle, \quad (13)$$

where I and J are operators which act in flavor and spin spaces, respectively, and the baryon states $|B\rangle$ are constructed in the framework of the SU(6) spin-flavor and SU(3) color symmetry. Analogously, for two-body operators, we have

$$\begin{aligned} & \chi_{f'}^\dagger \chi_{s'}^\dagger I_1^{f'f} J_1^{s's} \chi_s^\dagger \chi_f^\dagger \otimes \chi_{k'}^\dagger \chi_{\sigma'}^\dagger I_2^{k'k} J_2^{\sigma'\sigma} \chi_\sigma^\dagger \chi_k^\dagger \\ & \xrightarrow{\text{Proj.}} \langle B | \sum_{i \neq j}^3 (I_1 J_1)^{(i)} \otimes (I_2 J_2)^{(j)} | B \rangle. \end{aligned} \quad (14)$$

In Eq. (12), $\mathcal{L}_I^W(x)$ is the quark-meson interaction Lagrangian of the PCQM as given in Eq. (2), and the axial-vector

TABLE I. The energy levels of a single quark with $E_0 = 0.524$ GeV.

Notation	n	l	j	κ	E_α (GeV)
$1s_{1/2}$	1	0	$1/2$	-1	0.524
$2s_{1/2}$	2	0	$1/2$	-1	0.722
$3s_{1/2}$	3	0	$1/2$	-1	0.935
$4s_{1/2}$	4	0	$1/2$	-1	1.122
$1p_{1/2}$	1	1	$1/2$	1	0.669
$2p_{1/2}$	2	1	$1/2$	1	0.847
$3p_{1/2}$	3	1	$1/2$	1	1.041
$1p_{3/2}$	1	1	$3/2$	-2	0.738
$2p_{3/2}$	2	1	$3/2$	-2	0.877
$3p_{3/2}$	3	1	$3/2$	-2	1.059
$1d_{3/2}$	1	2	$3/2$	2	0.805
$2d_{3/2}$	2	2	$3/2$	2	1.009
$1d_{5/2}$	1	2	$5/2$	-3	0.844
$2d_{5/2}$	2	2	$5/2$	-3	1.025
$1f_{5/2}$	1	3	$5/2$	3	0.920
$2f_{5/2}$	2	3	$5/2$	3	1.101
$1f_{7/2}$	1	3	$7/2$	-4	0.933
$2f_{7/2}$	2	3	$7/2$	-4	1.133
$1g_{7/2}$	1	4	$7/2$	4	1.022
$1g_{9/2}$	1	4	$9/2$	-5	1.028

current operator A_i^μ takes the form

$$A_i^\mu = \bar{\psi} \gamma^\mu \gamma^5 \frac{\lambda_i}{2} \psi - \frac{f_{ijk}}{2F} \bar{\psi} \gamma^\mu \lambda_j \psi \Phi_k + \bar{\psi} (\hat{Z} - 1) \gamma^\mu \gamma^5 \frac{\lambda_i}{2} \psi + o(\Phi_i^2), \quad (15)$$

where the renormalization constant \hat{Z} is determined by the nucleon charge conservation condition. Following the renormalization technique set out in Refs. [42,43], we may derive in the present work the renormalization constant \hat{Z} with including the intermediate excited quark states

$$\hat{Z} = 1 - \frac{1}{3(4\pi F)^2} \sum_{\Phi, \alpha} \int_0^\infty dk \frac{a_\Phi k^4 \mathcal{F}_{\Phi NN}^\alpha(k)}{\omega_\Phi(k^2)[\omega_\Phi(k^2) + \Delta E_\alpha]^2}, \quad (16)$$

and the renormalized current quark masses \hat{m}^r

$$\hat{m}^r = 1 - \frac{1}{3\gamma(4\pi F)^2} \sum_{\Phi, \alpha} \int_0^\infty dk \frac{a_\Phi k^4 \mathcal{F}_{\Phi NN}^\alpha(k)}{\omega_\Phi(k^2)[\omega_\Phi(k^2) + \Delta E_\alpha]}, \quad (17)$$

where $\omega_\Phi(k^2) = \sqrt{M_\Phi^2 + k^2}$ and the constants $a_\pi = 9$, $a_K = 6$, and $a_\eta = 1$. The energy shift of a single quark $\Delta E_\alpha = E_\alpha - E_0$, and

$$\mathcal{F}_{\Phi NN}^\alpha(k) = F_{I\alpha}(k) F_{I\alpha}^\dagger(k) - 2\omega_\Phi(k^2) F_{I\alpha}(k) F_{II\alpha}^\dagger(k) + \omega_\Phi^2(k^2) F_{II\alpha}(k) F_{I\alpha}^\dagger(k), \quad (18)$$

$$F_{I\alpha}(k) = \int_0^\infty dr r^2 \int_\Omega d\Omega [g_0(r) g_\alpha(r) + f_0(r) f_\alpha(r) \cos 2\theta] e^{ikr \cos \theta} C_\alpha Y_{l_\alpha 0}(\theta, \phi), \quad (19)$$

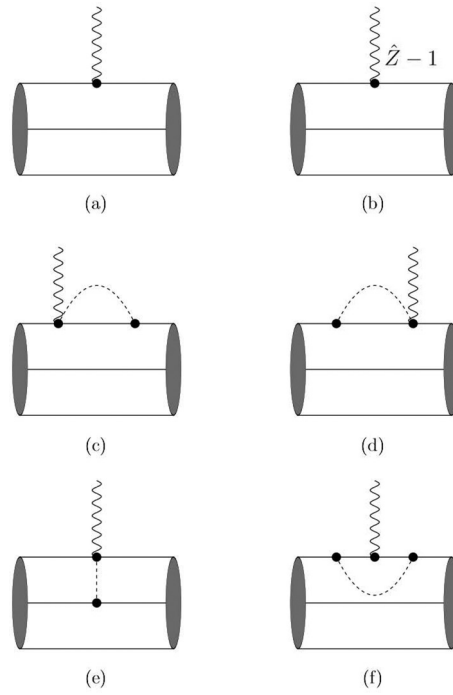


FIG. 3. Diagrams contributing to the axial form factor of octet baryons: $3q$ -core leading order (a), $3q$ -core counterterm (b), self-energy I (c), self-energy II (d), meson exchange (e), and vertex correction (f).

$$F_{II\alpha}(k) = \frac{i}{k} \int_0^\infty dr r^2 [g_0(r) f_\alpha(r) - g_\alpha(r) f_0(r)] \times \int_\Omega d\Omega \cos \theta e^{ikr \cos \theta} C_\alpha Y_{l_\alpha 0}(\theta, \phi). \quad (20)$$

Here, we let $g_0(r) = g_{1s_{1/2}}(r) C_0 Y_{00}(\theta, \phi)$ and $f_0(r) = f_{1s_{1/2}}(r) C_0 Y_{00}(\theta, \phi)$. The label $\alpha = (nl_\alpha jm)$ in the above equations characterizes the quark state. C_α in Eqs. (19) and (20) is the Clebsch-Gordan coefficients $C_\alpha = \langle l_\alpha 0 \frac{1}{2} \frac{1}{2} | j \frac{1}{2} \rangle$ and $Y_{l_\alpha 0}(\theta, \phi)$ is the usual spherical harmonics with l_α being the orbital quantum numbers of the intermediate states α . Extensive details of the renormalization technique could be found in Refs. [42,43].

In accordance with the $\mathcal{L}_I^W(x)$ in Eq. (2) and the A_i^μ in Eq. (15), there are six Feynman diagrams contributing to the axial charges of the octet and decuplet baryons and shown in Fig. 3. In order to evaluate the axial charges of Eq. (12), the confined quark field Feynmann propagator in Fig. 3 is defined

TABLE II. The constants c_i^B for the axial charges of the octet and decuplet baryons.

	N	Σ	Ξ	Δ	Σ^*	Ξ^*
c_1^B	$5/3$	$4/3$	$-1/3$	-3	-2	-1
c_2^B	$5/6$	$2/3$	$-1/6$	$-3/2$	-1	$-1/2$
c_3^B	8	0	0	0	0	0
c_4^B	0	4	-4	0	0	0
c_5^B	$-5/9$	$-4/9$	$1/9$	1	$2/3$	$1/3$

TABLE III. Numerical results for the octet and decuplet baryon axial charges g_A^B . The experimental data is taken from Ref. [1]. For comparison, the results from lattice-QCD with the chiral extrapolation [23], ChTP [29,30], and RCQM [41] are also compiled.

PCQM	Exp. [1]	Lattice QCD [23]	ChPT [29,30]	EGBE [41]	psGBE [41]	OGE [41]
g_A^N	1.263	1.2723 ± 0.0023	1.180 ± 0.100	1.18	1.15	1.15
g_A^Σ	0.896		0.900 ± 0.096	1.03 ^a	0.92 ^a	0.92 ^a
g_A^{Ξ}	-0.275		-0.277 ± 0.034	-0.23	-0.21	-0.22
g_A^Δ	-1.863			-2.24 ^b	-2.24 ^b	-2.15 ^b
$g_A^{\Sigma^*}$	-1.242				-1.50 ^a	-1.41 ^a
$g_A^{\Xi^*}$	-0.621				-0.75	-0.70

^aThis numerical result is adjusted by $\sqrt{2}$ due to the definition of g_A^Σ and $g_A^{\Sigma^*}$ in Refs. [30,41].

^bThis numerical result is adjusted by 2 due to the definition of g_A^Δ in Refs. [29,41].

as

$$iG_\psi(x, y) = \sum_\alpha u_\alpha(x)\bar{u}_\alpha(y)e^{-iE_\alpha(x_0 - y_0)}\theta(x_0 - y_0), \quad (21)$$

where $u_\alpha(x)$ are quark wave functions and have been obtained numerically as shown in Figs. 2(a)–2(k). In the present work, both the intermediate ground state $1s_{1/2}$ and the excited $1p_{1/2}$, $1p_{3/2}$, $1d_{3/2}$, $1d_{5/2}$, $1f_{5/2}$, $1f_{7/2}$, $2s_{1/2}$, $2p_{1/2}$, $2p_{3/2}$, and $3s_{1/2}$ quark states are included in the loop diagrams. For the mesons, the free Feynman propagator for a boson field is given by

$$i\Delta_{ij}(x, y) = \delta_{ij} \int \frac{d^4k}{(2\pi)^4 i} \frac{\exp[-ik(x - y)]}{M_\Phi^2 - k^2 - i\epsilon}. \quad (22)$$

The corresponding analytical expressions for the relevant diagrams are derived as follows:

(a) Leading order (LO) diagram:

$$g_A^B|_{LO} = c_1^B 2\pi \int_0^\infty dr r^2 \int_0^\pi d\theta \sin\theta \times [g_0(r)^2 + f_0(r)^2 \cos(2\theta)]. \quad (23)$$

(b) Three-quark core counterterm (CT) diagram:

$$g_A^B|_{CT} = (\hat{Z} - 1)g_A^B|_{LO}. \quad (24)$$

(c) Self-energy I (SE I) diagram:

$$g_A^B|_{SE:I} = -\frac{2}{(4\pi F)^2} \int_0^\infty dk \int_{-1}^1 dx k^4 \mathcal{F}_{\Phi\alpha}^B(k) \times [2(1-x^2)F_{III\alpha}(k) + (1-2x^2)F_{IV\alpha}(k)], \quad (25)$$

TABLE IV. Numerical results for axial charges g_A^B of octet and decuplet baryons separated into $3q$ core (LO) and meson cloud (Loop) contributions.

	$3q$ core	Meson	Total
g_A^N	0.883	0.380	1.263
g_A^Σ	0.707	0.189	0.896
g_A^{Ξ}	-0.177	-0.098	-0.275
g_A^Δ	-1.588	-0.275	-1.863
$g_A^{\Sigma^*}$	-1.059	-0.183	-1.242
$g_A^{\Xi^*}$	-0.530	-0.091	-0.621

where

$$\mathcal{F}_{\Phi\alpha}^B(k) = \frac{c_1^B(\omega_\pi(k^2)F_{II\alpha}(k) - F_{I\alpha}(k))}{\omega_\pi(k^2)(\omega_\pi(k^2) + \Delta E_\alpha)} + \frac{c_2^B(\omega_K(k^2)F_{II\alpha}(k) - F_{I\alpha}(k))}{\omega_K(k^2)(\omega_K(k^2) + \Delta E_\alpha)}, \quad (26)$$

$$F_{III\alpha}(k) = \frac{i}{k} \int_0^\infty dr r^2 g_0(r) f_\alpha(r) \int_\Omega d\Omega \cos\theta e^{ikr \cos\theta} C_\alpha Y_{l_\alpha 0}(\theta, \phi), \quad (27)$$

$$F_{IV\alpha}(k) = \frac{i}{k} \int_0^\infty dr r^2 [g_\alpha(r)f_0(r) - g_0(r)f_\alpha(r)] \int_\Omega d\Omega \cos\theta e^{ikr \cos\theta} C_\alpha Y_{l_\alpha 0}(\theta, \phi). \quad (28)$$

(d) Self-energy II (SE II) diagram:

$$g_A^B|_{SE:I} = g_A^B|_{SE:II}. \quad (29)$$

It is noted that the SE I and SE II diagrams lead to the same results based on the T symmetry.

(e) Meson exchange (EX) diagram:

$$g_A^B|_{EX} = -\frac{1}{(4\pi F)^2} \int_0^\infty dk k^4 \int_{-1}^1 dx (1-x^2) \times F_{I0}(k) F_{III0}(k) \left[\frac{c_3^B}{\omega_\pi^2(k^2)} + \frac{c_4^B}{\omega_K^2(k^2)} \right]. \quad (30)$$

TABLE V. Meson cloud contributions to axial charges g_A^B of octet and decuplet baryons derived with the ground-state and excited-state quark propagators, respectively.

	Ground	Excited	Total
g_A^N	0.418	-0.038	0.380
g_A^Σ	0.220	-0.031	0.189
g_A^{Ξ}	-0.106	0.008	-0.098
g_A^Δ	-0.343	0.068	-0.275
$g_A^{\Sigma^*}$	-0.229	0.046	-0.183
$g_A^{\Xi^*}$	-0.114	0.023	-0.091

(f) Vertex correction (VC) diagram:

$$g_A^B|_{VC} = \frac{1}{3(4\pi F)^2} \int_0^\infty dk k^4 \mathcal{F}_{\Phi\alpha\beta}^B(k) (\mathcal{A}_{\alpha\beta} + 2\mathcal{B}_{\alpha\beta} + \mathcal{C}_{\alpha\beta}), \quad (31)$$

with

$$\begin{aligned} \mathcal{F}_{\Phi\alpha\beta}^B(k) &= c_1^B \frac{F_{I\alpha}(k)F_{I\beta}^\dagger(k) - \omega_\pi(k^2)[F_{I\alpha}(k)F_{II\beta}^\dagger(k) + F_{II\alpha}(k)F_{I\beta}^\dagger(k)] + \omega_\pi^2(k^2)F_{II\alpha}(k)F_{II\beta}^\dagger(k)}{\omega_\pi(k^2)[\omega_\pi(k^2) + \Delta\mathcal{E}_\alpha][\omega_\pi(k^2) + \Delta\mathcal{E}_\beta]} \\ &\quad + c_5^B \frac{F_{I\alpha}(k)F_{I\beta}^\dagger(k) - \omega_\eta(k^2)[F_{I\alpha}(k)F_{II\beta}^\dagger(k) + F_{II\alpha}(k)F_{I\beta}^\dagger(k)] + \omega_\eta^2(k^2)F_{II\alpha}(k)F_{II\beta}^\dagger(k)}{\omega_\eta(k^2)[\omega_\eta(k^2) + \Delta\mathcal{E}_\alpha][\omega_\eta(k^2) + \Delta\mathcal{E}_\beta]}, \end{aligned} \quad (32)$$

$$\mathcal{A}_{\alpha\beta} = \int_0^\infty dr r^2 [g_\alpha(r)g_\beta(r) - f_\alpha(r)f_\beta(r)] \int_\Omega d\Omega [C_\alpha C_\beta Y_{l_\alpha 0}(\theta, \phi)Y_{l_\beta 0}(\theta, \phi) - D_\alpha D_\beta Y_{l_\alpha 1}^*(\theta, \phi)Y_{l_\beta 1}(\theta, \phi)], \quad (33)$$

$$\mathcal{B}_{\alpha\beta} = \int_0^\infty dr r^2 f_\alpha(r)f_\beta(r) \int_\Omega d\Omega \cos^2 \theta [C_\alpha C_\beta Y_{l_\alpha 0}(\theta, \phi)Y_{l_\beta 0}(\theta, \phi) - D_\alpha D_\beta Y_{l_\alpha 1}^*(\theta, \phi)Y_{l_\beta 1}(\theta, \phi)], \quad (34)$$

$$\mathcal{C}_{\alpha\beta} = \int_0^\infty dr r^2 f_\alpha(r)f_\beta(r) \int_\Omega d\Omega \cos 2\theta [C_\alpha D_\beta Y_{l_\alpha 0}(\theta, \phi)Y_{l_\beta 1}(\theta, \phi)e^{-i\phi} + D_\alpha C_\beta Y_{l_\alpha 1}^*(\theta, \phi)Y_{l_\beta 0}(\theta, \phi)e^{i\phi}], \quad (35)$$

where $D_\alpha = \langle l_\alpha 1\frac{1}{2} - \frac{1}{2}|j\frac{1}{2}\rangle$.

The constants c_i^B listed in Table II are the matrix elements of the flavor and spin operators between baryon states and are evaluated by employing projection technique, namely, the constants c_1^B , c_2^B , and c_5^B are from Eq. (13) while two-body projection Eq. (14) results in the constants c_3^B and c_4^B . Next, we evaluate the axial charges of the octet and decuplet baryons while including both the ground and excited states in the quark propagator. It is noted that there is not any free parameter in the following numerical calculations.

In Table III, we present the PCQM numerical values of the octet and decuplet baryons axial charges and also compile the results from the lattice QCD [23], ChTP [29,30], and RCQM [41] for comparison. To make it easier for comparison, we have adjusted the results of Refs. [29,30,41] due to another definition of g_A^B as mentioned in Table III. It is clear that the PCQM result of g_A^N is consistent with experimental value, while g_A^N from lattice QCD and other approaches are smaller than the PCQM one. For Σ and Ξ hyperons, the PCQM predictions are very close to lattice QCD measurements with chiral extrapolation at the physical m_π point, and the PCQM also yields very similar results with ChTP and RCQM for g_A^Σ and g_A^Ξ . Based on coefficients c_3^B and c_4^B in Table II, the EX diagram in Fig. 3 does not contribute to axial charges of decuplet baryons. Thus the PCQM predictions on decuplet baryons (g_A^Δ , $g_A^{\Sigma^*}$, and $g_A^{\Xi^*}$) are below the RCQM results [41] as shown in Table III.

Moreover, the numerical results of g_A^B are separated into $3q$ -core (LO) and meson cloud (loop) contributions and listed in Table IV. It is found that the meson cloud plays an important role in the axial charge g_A^B of octet and decuplet baryons, contributing around 30% to the total values, and the similar effects have been also observed in other frameworks [6,39].

In the work, we have calculated g_A^B by including both the ground $1s_{1/2}$ and excited $1p_{1/2}$, $1p_{3/2}$, $1d_{3/2}$, $1d_{5/2}$, $1f_{5/2}$, $1f_{7/2}$, $2s_{1/2}$, $2p_{1/2}$, $2p_{3/2}$, and $3s_{1/2}$ states in the quark propagator in Figs. 3(c), 3(d), and 3(f). To illustrate the effect of excited intermediate quark states, we give separately in Table V the meson cloud contributions from Figs. 3(c), 3(d), and 3(f) with

the ground-state as well as excited-state quark propagators. The results in Table V reveal that the meson cloud contribution to g_A^B stems mainly from the diagrams with the ground-state quark propagator while the excited intermediate quark states reduce g_A^B by 10–20%.

IV. SUMMARY AND CONCLUSIONS

In this work, the axial charges of octet and decuplet baryons in the PCQM are evaluated with considering the quark propagator with both the ground $1s_{1/2}$ and excited $1p_{1/2}$, $1p_{3/2}$, $1d_{3/2}$, $1d_{5/2}$, $1f_{5/2}$, $1f_{7/2}$, $2s_{1/2}$, $2p_{1/2}$, $2p_{3/2}$, and $3s_{1/2}$ states, in which the excited quark states have been derived in our previous work [58] by solving the Dirac equation with the Cornell-like PCQM potential extracted in accordance with the predetermined ground-state quark wave function. It is noted that there is no any free parameter in the present work. We find that the PCQM result on g_A^N is consistent with experimental value, and predictions on hyperons g_A^Σ and g_A^Ξ are very closed to lattice QCD values. But our predictions of decuplet baryons g_A^Δ , $g_A^{\Sigma^*}$, and $g_A^{\Xi^*}$ are smaller than ones from the RCQM. In addition, the study reveals that the meson cloud is influential in the PCQM and contributes around 30% to the total values of g_A^B , which is similar to the findings of Refs. [6,39]. Also, we may conclude that the meson cloud contribution to g_A^B stems mainly from the processes in Figs. 3(c), 3(d), and 3(f) with the ground-state quark propagator while the excited intermediate quark states may reduce g_A^B by 10–20%.

ACKNOWLEDGMENTS

This work is supported by National Natural Science Foundation of China (Project No. 11547182), the Office of the Higher Education Commission under the NRU project of Thailand (SUT-CHE-NRU FtR 09/2561), and Thailand Research Fund (MRG5980255). X.L. and A.L. acknowledge support from Suranaree University of Technology.

- [1] C. Patrignani *et al.* (Particle Data Group), *Chin. Phys. C* **40**, 100001 (2016).
- [2] M. A. Morgan, G. A. Miller, and A. W. Thomas, *Phys. Rev. D* **33**, 817 (1986).
- [3] L. Y. Glozman, M. Radici, R. F. Wagenbrunn, S. Boffi, W. Klink, and W. Plessas, *Phys. Lett. B* **516**, 183 (2001).
- [4] S. Boffi, L. Y. Glozman, W. Klink, W. Plessas, M. Radici, and R. F. Wagenbrunn, *Eur. Phys. J. A* **14**, 17 (2002).
- [5] D. Merten, U. Loring, K. Kretzschmar, B. Metsch, and H. R. Petry, *Eur. Phys. J. A* **14**, 477 (2002).
- [6] J. Franklin, *Phys. Rev. D* **66**, 033010 (2002).
- [7] D. Dolgov, R. Brower, S. Capitani, P. Dreher, J. W. Negele, A. Pochinsky, D. B. Renner, N. Eicker, T. Lippert, K. Schilling, R. G. Edwards, and U. M. Heller (LHPC and SESAM Collaborations), *Phys. Rev. D* **66**, 034506 (2002).
- [8] D. Barquilla-Cano, A. J. Buchmann, and E. Hernandez, *Nucl. Phys. A* **714**, 611 (2003).
- [9] B. Julia-Diaz, D. O. Riska, and F. Coester, *Phys. Rev. C* **69**, 035212 (2004).
- [10] A. Ali Khan, M. Göckeler, P. Hägler, T. R. Hemmert, R. Horsley, D. Pleiter, P. E. L. Rakow, A. Schäfer, G. Schierholz, T. Wollenweber, and J. M. Zanotti (QCDSF Collaboration), *Phys. Rev. D* **74**, 094508 (2006).
- [11] M. R. Schindler, T. Fuchs, J. Gegelia, and S. Scherer, *Phys. Rev. C* **75**, 025202 (2007).
- [12] S. Sasaki, K. Orginos, S. Ohta, and T. Blum (RIKEN-BNL-Columbia-KEK Collaboration), *Phys. Rev. D* **68**, 054509 (2003).
- [13] R. G. Edwards *et al.* (LHPC Collaboration), *Phys. Rev. Lett.* **96**, 052001 (2006).
- [14] T. Yamazaki *et al.* (RBC+UKQCD Collaboration), *Phys. Rev. Lett.* **100**, 171602 (2008).
- [15] C. Alexandrou *et al.* (ETM Collaboration), *Phys. Rev. D* **83**, 045010 (2011).
- [16] R. Horsley, Y. Nakamura, A. Nobile, P. E. L. Rakow, G. Schierholz, and J. M. Zanotti, *Phys. Lett. B* **732**, 41 (2014).
- [17] T. Bhattacharya *et al.* (PNDME Collaboration), *Phys. Rev. D* **89**, 094502 (2014).
- [18] L. E. V. Bernard and U. G. Meißner, *J. Phys. G: Nucl. Part. Phys.* **28**, R1 (2002).
- [19] E. J. Beise, *Eur. Phys. J. A* **24S2**, 43 (2005).
- [20] M. R. Schindler and S. Scherer, *Eur. Phys. J. A* **32**, 429 (2007).
- [21] T. T. Takahashi and T. Kunihiro, *Phys. Rev. D* **78**, 011503 (2008).
- [22] H. W. Lin, T. Blum, S. Ohta, S. Sasaki, and T. Yamazaki, *Phys. Rev. D* **78**, 014505 (2008).
- [23] H. W. Lin and K. Orginos, *Phys. Rev. D* **79**, 034507 (2009).
- [24] S. Sasaki and T. Yamazaki, *Phys. Rev. D* **79**, 074508 (2009).
- [25] G. Erkol, M. Oka, and T. T. Takahashi, *Phys. Lett. B* **686**, 36 (2010).
- [26] M. J. Savage and J. Walden, *Phys. Rev. D* **55**, 5376 (1997).
- [27] R. Flores-Mendieta, E. E. Jenkins, and A. V. Manohar, *Phys. Rev. D* **58**, 094028 (1998).
- [28] M. Procura, B. U. Musch, T. R. Hemmert, and W. Weise, *Phys. Rev. D* **75**, 014503 (2007).
- [29] F. J. Jiang and B. C. Tiburzi, *Phys. Rev. D* **78**, 017504 (2008).
- [30] F. J. Jiang and B. C. Tiburzi, *Phys. Rev. D* **80**, 077501 (2009).
- [31] M. E. Carrillo-Serrano, I. C. Cloët, and A. W. Thomas, *Phys. Rev. C* **90**, 064316 (2014).
- [32] T. Ledwig, J. M. Camalich, L. S. Geng, and M. J. V. Vacas, *Phys. Rev. D* **90**, 054502 (2014).
- [33] G. Erkol and A. Ozpineci, *Phys. Rev. D* **83**, 114022 (2011).
- [34] F. Schlumpf, *Phys. Rev. D* **47**, 4114 (1993).
- [35] T. Ledwig, A. Silva, H. C. Kim, and K. Goeke, *JHEP* **07** (2008) 132.
- [36] C. Lorce, *Phys. Rev. D* **78**, 034001 (2008).
- [37] H. Dahiya and M. Randhawa, *Phys. Rev. D* **90**, 074001 (2014).
- [38] G. S. Yang and H. C. Kim, *Phys. Rev. C* **92**, 035206 (2015).
- [39] G. Ramalho and K. Tsushima, *Phys. Rev. D* **94**, 014001 (2016).
- [40] K.-S. Choi, W. Plessas, and R. F. Wagenbrunn, *Phys. Rev. C* **81**, 028201 (2010).
- [41] K.-S. Choi, W. Plessas, and R. F. Wagenbrunn, *Phys. Rev. D* **82**, 014007 (2010).
- [42] V. E. Lyubovitskij, T. Gutsche, A. Faessler, and E. G. Drukarev, *Phys. Rev. D* **63**, 054026 (2001).
- [43] V. E. Lyubovitskij, T. Gutsche, and A. Faessler, *Phys. Rev. C* **64**, 065203 (2001).
- [44] V. E. Lyubovitskij, T. Gutsche, A. Faessler, and M. R. Vinh, *Phys. Lett. B* **520**, 204 (2002).
- [45] V. E. Lyubovitskij, T. Gutsche, A. Faessler, and R. Vinh Mau, *Phys. Rev. C* **65**, 025202 (2002).
- [46] V. E. Lyubovitskij, P. Wang, T. Gutsche, and A. Faessler, *Phys. Rev. C* **66**, 055204 (2002).
- [47] K. Pumsa-ard, V. E. Lyubovitskij, T. Gutsche, A. Faessler, and S. Cheedket, *Phys. Rev. C* **68**, 015205 (2003).
- [48] K. Khosonthongkee, V. E. Lyubovitskij, T. Gutsche, A. Faessler, K. Pumsaard, S. Cheedket, and Y. Yan, *J. Phys. G: Nucl. Part. Phys.* **30**, 793 (2004).
- [49] T. Inoue, V. E. Lyubovitskij, T. Gutsche, and A. Faessler, *Phys. Rev. C* **69**, 035207 (2004).
- [50] S. Cheedket, V. E. Lyubovitskij, T. Gutsche, A. Faessler, K. Pumsa-ard, and Y. Yan, *Eur. Phys. J. A* **20**, 317 (2004).
- [51] T. Inoue, V. E. Lyubovitskij, T. Gutsche, and A. Faessler, *Int. J. Mod. Phys. E* **14**, 995 (2005).
- [52] T. Inoue, V. E. Lyubovitskij, T. Gutsche, and A. Faessler, *Int. J. Mod. Phys. E* **15**, 121 (2006).
- [53] Y. Dong, A. Faessler, T. Gutsche, J. Kuckei, V. E. Lyubovitskij, K. Pumsa-ard, and P. Shen, *J. Phys. G* **32**, 203 (2006).
- [54] C. Dib, A. Faessler, T. Gutsche, S. Kovalenko, J. Kuckei, V. E. Lyubovitskij, and K. Pumsa-ard, *J. Phys. G* **32**, 547 (2006).
- [55] A. Faessler, T. Gutsche, V. E. Lyubovitskij, and C. Oonariya, *J. Phys. G* **35**, 025005 (2008).
- [56] X. Y. Liu, K. Khosonthongkee, A. Limphirat, and Y. Yan, *J. Phys. G: Nucl. Part. Phys.* **41**, 055008 (2014).
- [57] X. Y. Liu, K. Khosonthongkee, A. Limphirat, P. Suebka, and Y. Yan, *Phys. Rev. D* **91**, 034022 (2015).
- [58] X. Y. Liu, D. Smart, Y. J. Gao, K. Khosonthongkee, A. Limphirat, and Y. Yan, *arXiv:1707.02536* [hep-ph] (unpublished).
- [59] X. Y. Liu, Z. J. Liu, A. Limphirat, K. Khosonthongkee, and Y. Yan, *Ann. Phys.* **388**, 114 (2018).